Water Cerenkov muon detector near the Angra-II reactor core: the hardware.

A. F. Barbosa[∗]**, R. Machado, A. Vilar, A. Schiappacassa, R. G. Gama, L. M. de Andrade Filho, H. P. Lima Junior**

Centro Brasileiro de Pesquisas Fsicas - CBPF, e-mail: laudo@cbpf.br

G. P. Guedes

Universidade Estadual de Feira de Santana - UEFS

Abstract

We report the installation, near the Angra-II nuclear reactor, of a cosmic muons detector based on the Cerenkov effect in a water tank. The hardware components are described. In addition to details related to the detector design, the description includes the analog signal processing modules and the data acquisition interface to a personal computer. The former includes a pre-amplifier, a leading-edge discriminator, a rate meter, and a temperature sensing circuit. The latter makes use of a general purpose device named Data Processing Module (DPM), which is here programmed to perform the required operations. Characterization data for every unit are also presented.

[∗]Corresponding author, e-mail: laudo@cbpf.br

1   Introduction

An important milestone for the Angra Neutrinos Project has been reached in the year 2008: the installation of a laboratory container upon the Angra-II dome outer wall. Besides the fact that this represents the first visible indications of the neutrino detector implementation in the Angra nuclear power plant area, the laboratory container opens new trends impacting the detector concept itself. The main reason for that is the fact that the laboratory is placed as close as possible to the reactor core ($\approx 25m$ distance). As a consequence, the highest possible flux of anti-neutrinos per unit volume is available inside the container. It is therefore natural to investigate neutrino detection techniques that could be implemented in this laboratory and comply with the power plant safety rules and policies. In particular, the adopted technique should not require the construction of a deep underground shaft for shielding purposes. One of the basic concerns in this direction is the background of particles impinging the detector volume, which has to be understood and vetoed. A water Cerenkov detector tank has then been installed in the container for starting a detailed monitoring of these particles.

The present note describes the detector design and its associated data acquisition system in the hardware level. The data acquisition software is the object of another note. It may be emphasized that this achievement not only provides a helpful tool for studying the background radiation, but also permits us to establish important aspects of the future neutrino detection facility, as for example the online data transmission from Angra to other participating institutions.

2   The water Cerenkov detector

The electric field of a charged particle polarizes the molecules composing the material through which this particle travels. The polarization is a local effect, so that it ceases when the particle moves away from the considered spatial position and there is, therefore, spatial charge variation due to the particle passage. Since electric charge variation gives rise to radiation emission, radiation is likely to accompany the passage of a particle in a dielectric medium. This is illustrated in Figure 1. Although the referred polarization is a tiny effect, depending on the speed of the particle there can be constructive interference of the radiation emission wavefront, in which case the radiation may be easily observed. Such is the case when the particle speed is extremely high, exceeding the speed of light in the medium.

A simple and intuitive treatment of the phenomenon allows one to determine some of the relevant physical parameters. As shown in Figure 2, when the particle speed is much lower than the speed of light in the medium (given by c/n, where c is the speed of light in vacuum and n is the refractive index of the medium), the emitted radiation wavefront is ahead of the particle and there is no possibility for constructive interference. It may also be noted that, in this case, the net resulting polarization of the dielectric along the particle direction is negligible (see Figure 1). On the other hand, if the particle speed is much higher than c/n, constructive interference takes place and there may be an observable amount of radiation around an angle θ respective to the particle direction.

After a time interval Δt measured from the instant when the particle reaches position a, the particle will have moved to position b. The corresponding distance is given by $v.\Delta t$, where v is the particle speed. In the same time interval, the emitted radiation wavefront will have traveled the distance $c.\Delta t/n$. At this instant, in the case of highly relativistic particles, the wavefronts emitted before Δt will interfere constructively and yield maximum light intensity along the direction $a - c$ defined by an angle θ relative to the $a - b$ segment. This angle is expressed by:
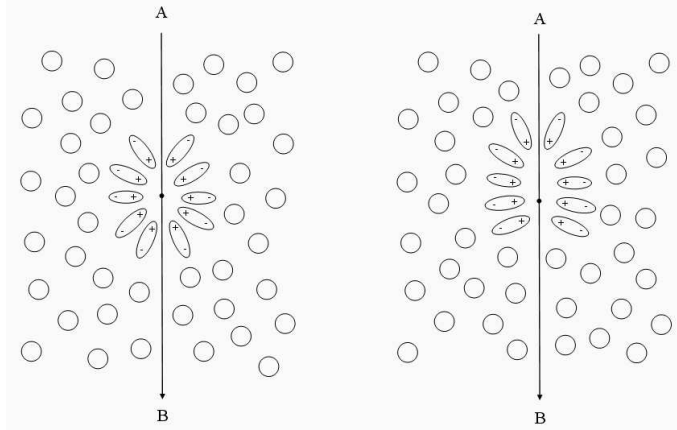
Figure 1: Schematic instantaneous representation of the polarization effect due to the movement of a negatively charged particle along the direction AB in a dielectric medium, with speed $< c/n$ (on the left) and $> c/n$ (on the right), where c us the speed of light in vacuum and n is the refractive index.
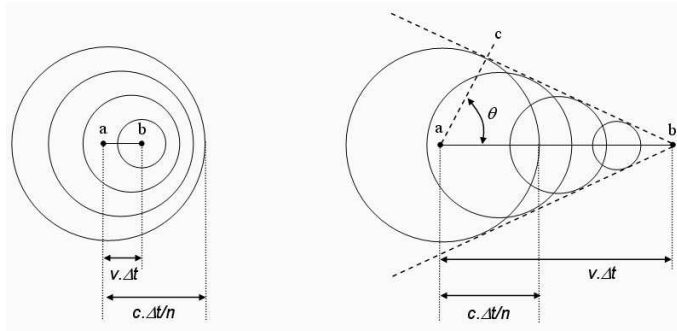

Figure 2: Representation of the emitted radiation wavefront for a charged particle when its speed is $< c/n$ (on the left) and $> c/n$ (on the right). There is constructive interference of the wavefronts in the latter case.

$$\cos\theta = \frac{\frac{c}{n}\Delta t}{\beta c \Delta t} = \frac{1}{\beta n} \tag{1}$$

According to Eq. 1, we see that there is a minimum particle speed for which the Cerenkov effect starts to be observable (that means: $\theta > 0$). This speed is given by $\beta_{min} = 1/n$. There is as well a maximum angle, θ_{max}, for radiation emission, given by the condition $\beta \leq 1$. Considering water as the dielectric medium, with $n = 1.33$, we find: $\beta_{min} = 0.75$ and $\theta_{max} = 41^o$. A more detailed treatment of the Cerenkov effect may be found in references [1][2]. In particular, taking the energy of a radiated photon as $h\nu$ - where ν is the light wave frequency and h is the Planck constant - it may be estimated from Maxwell equations that the number of photons radiated by the Cerenkov process per unit length of radiator medium, in the bandwidth comprised from wavelengths λ_1 to λ_2, is given by [2]:

$$N(\lambda_1, \lambda_2) = \frac{2\pi q^2}{\hbar c}\left(1 - \frac{1}{\beta^2 \varepsilon}\right)\left(\frac{1}{\lambda_1} - \frac{1}{\lambda_2}\right) \tag{2}$$

In Eq. 2, q is the particle electric charge, $\hbar = h/2\pi$ and ε is the dielectric constant (supposed to be constant in the considered bandwidth). If we take $\lambda_2 - \lambda_1 = \Delta\lambda$ and let $\lambda_1 \equiv \lambda$, Eq. 2 leads to:

$$N(\lambda_1, \lambda_2) = N(\lambda) \simeq \frac{\Delta\lambda}{\lambda(\lambda + \Delta\lambda)} \tag{3}$$

In Figure 3 we plot $N(\lambda)$ from Eq. 3, with $\Delta\lambda = 1nm$ and λ covering the visible light spectrum. The Cerenkov light yield is seen to be negligible at high wavelengths. It has to be noticed that there is also a limit for low wavelengths, not taken into account by Maxwell equations: the radiated light wavelength is not expected to be shorter than the particle dimensions, nor should it correspond to a photon energy comparable to the energy of the particle itself.
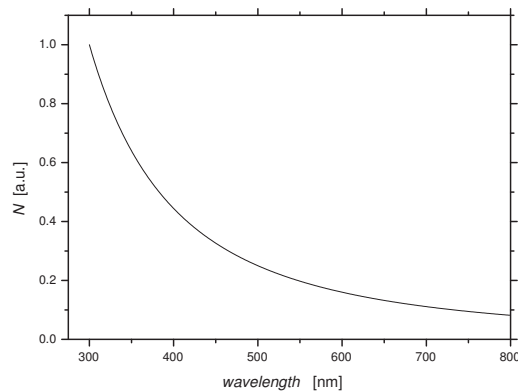

Figure 3: Cerenkov effect light yield as a function of the wavelength

2.1 The detector design

From the discussion above, we conclude that the detection of relativistic charged particles may be obtained from the observation of Cerenkov light. In order to obtain such a detector, the main ingredients are the radiator and the light sensor. One of the simplest radiators that we may think of is water. For the light sensors, photomultiplier (PMT) tubes are known to be very sensitive devices, generating an electric pulse for single photons absorbed in a photocathode. This combination, water as radiator and PMT as light sensor, has been adopted for the detection of cosmic muons in the laboratory container near the Angra-II reactor core.

This approach has been tested since long ago (*e.g.* [3]) and is also used in modern experiments (*e.g.* [4]). Since these detectors are typically expected to operate over several years, special care must be taken to purify the water, so that the probability for biological material to develop and thus interfere on the light yield stability is reduced to minimum. The usual parameter to quantify this probability is the Total Organic Carbon (TOC). Actually, carbon is the basic food for micro-organisms, and its availability in water may be correlated to the probability for biological material to spread as, for example, bacteria colonies. Besides, the optical transparency has also to be taken care of, since photons generated by the Cerenkov effect have to find their way to the PMTs. The transparency is mainly related to the presence of minerals, and the overall effect is quantified by the electrical resistivity per unit length of water. We have had the opportunity to use water of excellent quality produced by Eletronuclear, the agency in charge of operating the Angra nuclear power complex. This water is used in the primary circuit of the nuclear reactor, and has to be very close to 100% free of contaminants that could become radioisotopes. It is then subject to constraints that naturally comply with those of a Cerenkov detector. The water quality parameters are shown in Table 1.

Parameter	Value
TOC	$\approx 120\ ppb$
Conductivity	$\approx 2.5\ M\Omega$
Sodium content	$\approx 0.4\ ppb$
Silicon content	$\approx 15\ ppb$
Chloride content	$\approx 1\ ppb$

Table 1: Water quality parameters

The currently used PMT has a flat 5" diameter photocathode which is placed directly in contact with the water surface. It is powered with a voltage divider that distributes the operating voltage to each of the PMT dynodes up to a maximum of $2000V$. At this voltage the gain is around 10^5 - a relatively low gain compared to other typical PMTs, but enough to observe cosmic muons crossing the water volume. The complete diagram of the detector parts is shown in Figure 4.
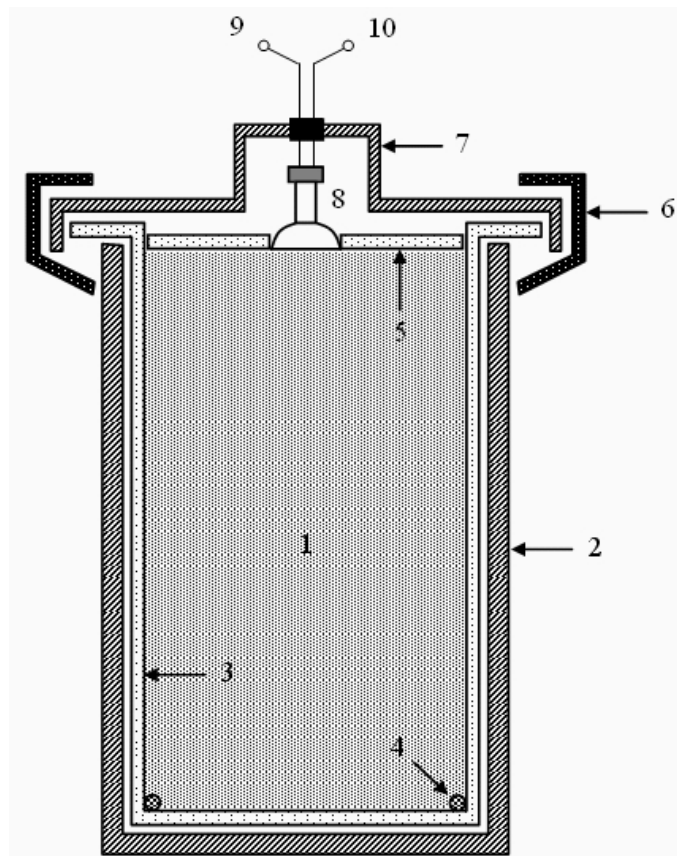

Figure 4: Detector schematic diagram showing: 1-water, 2-tank, 3-Tyvek bag, 4-bag holder, 5-Tyvek top cover, 6-black rubber sealing, 7-tank hat, 8-PMT + base, 9-high voltage supply, 10-signal output.

The water is contained by a black resin plastic tank in the volume of a cylinder with $1.28m$ height and $0.8m$ diameter. The inner walls of the tank are covered by a bag made with white Tyvek, which has the property of diffusely reflecting light of wavelength near the UV band. The PMT is placed at the top of the tank, directly touching the water surface. A hat covers the PMT and the tank top. External light is shielded by the materials composing the tank and the hat. Eventual leaks through the interface between them is shielded by a black rubber strap that tightly holds them together. It may be

seen from the drawing that a crossing relativistic muon will produce Cerenkov light in the water; most of this light bounces at the Tyvek covered walls and is eventually captured by the PMT and produces an electric signal. A feed-through implemented at the hat top allows the powering of the PMT with high voltage and the transmission of the output signal. The expected number of Cerenkov photons per unit length of radiator crossed by a cosmic muon has to be evaluated taking into account the light yield expressed by Eq. 2 as well as other physical parameters related to the practical implementation, such as: the PMT photocathode quantum efficiency (typically in the range of 10%), the water transparency, the reflectivity of the detector inner walls, the front-end electronics gain. We may roughly estimate (See [3][5]) that a relativistic muon traversing $1m$ water length produces $\approx 10^2 - 10^3$ Cerenkov photons, which are finally converted into $\approx 10 - 10^2$ photoelectrons in the PMT photocathode.

3   Electronics

The electric pulse resulting at the PMT output from the detection of a cosmic muon is usually a fast and low amplitude signal. The time development of the signal is related to the process of electron multiplication taking place in the PMT dynodes. For the relatively big PMTs such as the one that we use in the Cerenkov detector, the pulse duration is in the range of few tens of nanoseconds. Concerning the pulse amplitude, if we take, as a realistic estimate, 10 photoelectrons per detected muon and a PMT gain factor of 10^5, we are led to $0.16pC$ net charge available per event. Supposing that this charge is contained in a $10ns$ time bin and is delivered to the front-end electronics via a 50Ω terminated cable, we find that the corresponding pulse amplitude is $0.8mV$. This pulse has to be amplified and shaped, so that it may be analyzed under standard data acquisition techniques.

3.1   The analog signal processing modules

The amplifier and shaping circuit, shown in Figure 5, is the first module in the analog signal processing chain. It is basically the same circuit previously reported in [6], where simulation results were presented. It is composed by two main stages, the first of which provides an output signal proportional to the integral of the input signal, hence to the electric charge associated to the detected event. The second stage is simply a relatively low gain amplifier. Both stages make use of standard configurations of operational amplifiers. The $OPA657$ operational amplifier has been chosen since it provides the expected performance for the present application, including wide band, low offsets and good noise figure. In addition to the main stages, an RC filtering cell with variable R value is introduced in-between, so that the shape of the output signal is tuned to the analog-to-digital conversion sampling rate. An extra LC filtering stage is implemented at the output to filter out frequency components outside the signal bandwidth. The LC cell characteristic impedance is matched to the input impedance of the following stage (50Ω). This circuit may be used as an inverting or non-inverting unit, depending on which of the two inputs is enabled. Whichever one is chosen, the other one has to be grounded. The output is split in two paths: one of these takes the signal to the digitalization stage, the other one is used in the counting rate measurement.

The amplifier and shaping circuit provides the electric signal that may be digitalized and processed in the digital processing chain. From this, most of the quantitative information from the detector is made available. However, we also require two other features to be recorded during data acquisition: the events count rate and the local temperature. These may help doing better data analysis. Although the count rate may be off line estimated, it is preferable, in some cases, to have an independent
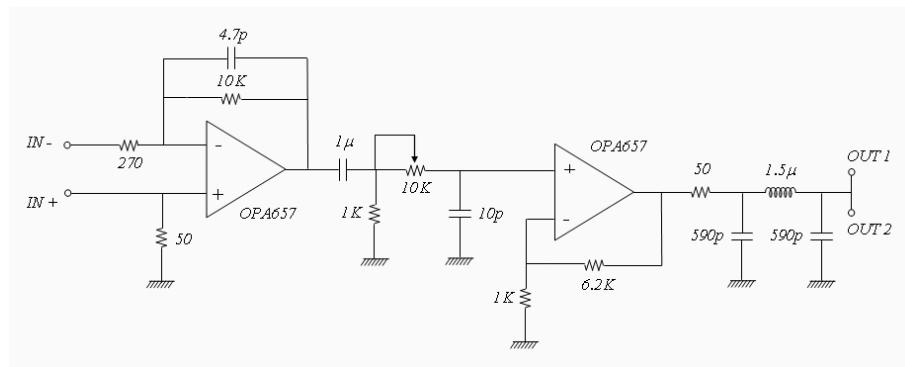
Figure 5: The amplifier and shaping circuit.

electronic channel exclusively dedicated to do this measurement. In Figure 6 is shown the circuit implemented for this purpose.
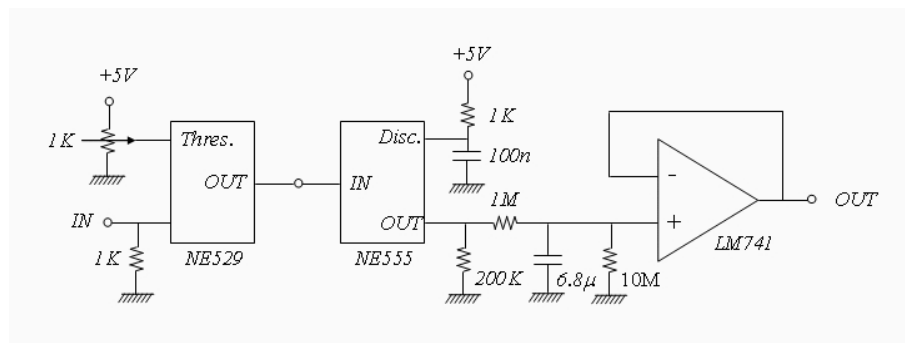

Figure 6: Discriminator + rate meter circuit.

In order to evaluate only the count rate, regardless of other parameters such as pulse amplitude and shape (thus, regardless of event energy), we have to generate and count a standard pulse for every detected event. In our approach, we first use a leading edge discriminator based on a fast comparator ($NE529$), with threshold level set as close as possible to the electronic noise. At this stage, a digital pulse is available at the output, but its time width depends on the input pulse amplitude. The next stage is therefore a mono-stable circuit based on a well known integrated circuit ($NE555$), whose role is to provide a fixed-width and fixed-amplitude pulse for a varying input pulse. The main elements responsible for this are a resistor and a capacitor externally added to the integrated circuit; the RC product defines the output signal width, while the amplitude is fixed by the circuit polarization. Since the expected counting rate is in the range of few KHz, the output pulse width is fixed to $\approx 100\mu s$, so that DC level variations corresponding to counting rate fluctuations lie well within the analog-to-digital conversion range (See §3.3). The last stage of this circuit includes passive signal integration at a time constant of few seconds (adjusted by another RC product: $1M\Omega \times 6.8\mu F$), followed by an active driver provided by a standard ($LF411$) operational amplifier. Since the integration time constant is much bigger than the expected time interval between detected events, the driver circuit output is simply a DC voltage level proportional to the events counting rate.

Temperature monitoring is important mainly to provide a data stream that correlates with the detector performance (the PMT and other detector components behavior depend on temperature). The temperature monitoring circuit is a very simple one, shown in Figure 7. It makes use of a thermistor,
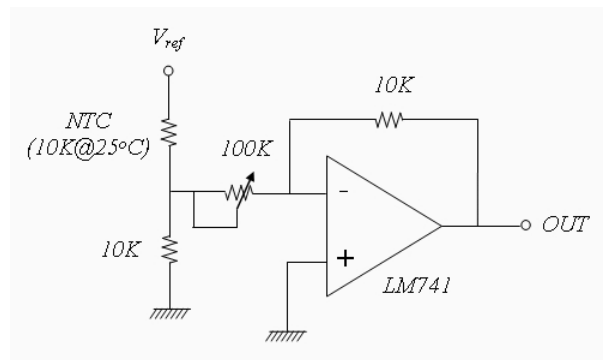
Figure 7: Temperature sensor circuit.

whose electric resistance is $10K\Omega$ @ 25^oC. The used thermistor does not feature excellent sensitivity over a wide temperature range, but it is reasonably linear a few degrees around the typical room temperature, and this is enough for the required application. As can be seen in Figure 7, the thermistor is used in a voltage divider, the output of which therefore depends on temperature. An attenuating circuit, also based on a standard operational amplifier configuration, is used to provide a DC level proportional to temperature and within the ADC conversion range (see §3.2). The reference voltage V_{ref} used in the temperature sensitive voltage divider is set to a negative value, so that, since the attenuator is an inverting circuit, the output is a positive DC level that rises with temperature.

The three circuits (front-end pre-amplifier, rate-meter and temperature sensor) have been mounted in a single printed circuit board and implemented inside a NIM standard mechanical box. This choice takes benefit of the low voltage power supplies available with the NIM standard electronic crates.

3.2 The digital signal processing module

The Digital Processing Module (DPM) is a custom system including hardware and software, designed to provide two basic types of measurements - amplitude and time intervals. The DPM offers a total of 28 channels, in the following distribution:

- Four input channels for amplitude measurement (analog signals);

- Eight input channels for time measurement (digital pulses);

- Twenty four input/output general-purpose channels (digital pulses).

A picture of one DPM unit is shown in Figure 8. The amplitude measurement is based on multistage differential pipelined analog-to-digital converters that digitize the input signals at a rate of 60 million samples per second (60 MSPS). The ADC resolution is 12 bits and its bipolar dynamic range is $2V$ peak to peak, providing an amplitude resolution close to 0.5 mV. The input channel circuit has a 50Ω termination resistor in the DPM, so that the input signal should preferably be taken from a driver with 50Ω output impedance.

The time interval between pulses is measured with a commercial time-to-digital (TDC) integrated circuit in common START mode, which means that one START input is the reference for the eight channels, called STOP's. The time resolution for these channels is $120ps$ and the maximum event rate is 2 million time-to-digital conversions per second. The dynamic range is $5ns$ to $7.8s$. Both the time-measurement inputs and the 24 general-purpose I/O's are TTL or LVTTL, compatible.
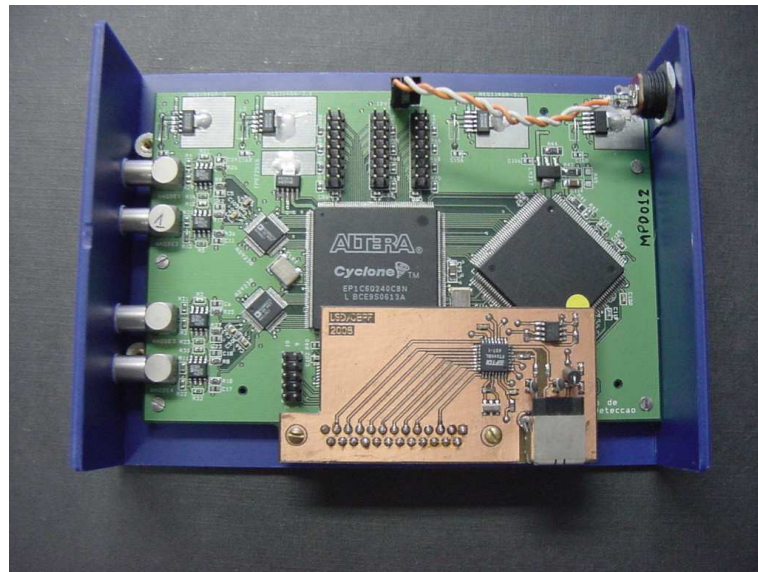
Figure 8: DPM picture showing the circuit components

A programmable logic device (Field Programmable Gate Array - FPGA) is the main processor in the module, being responsible for all the digital signal processing and for implementing the communication with personal computers through the Universal Serial Bus (USB) ports.

Concerning the firmware developed for the present application, three of the analog input channels have been enabled:

1. channel 1: receives and digitizes the PMT signal coming from the front-end amplifier;

2. channel 2: used to digitize the output of the rate-meter circuit;

3. channel 3: used to digitize the output of the temperature sensor circuit.

The TDC channels are therefore not enabled in the configuration used for the Cerenkov detector data acquisition. Triggering is enabled only on channel 1, with two modes of trigger available: internal and external. In the internal trigger mode, all the signals (channels 1, 2 and 3) are stored for further processing if the amplitude of the incoming signal on channel 1 is above (positive trigger) or below (negative trigger) a specific threshold defined in a programmable control register. Data is read in the following way: 32 samples before the trigger instant and 96 samples after, giving a total of 128 waveform samples per event. When using the DPM in the external trigger mode, one of the 24 general I/O channels is configured as a trigger input. In this case, data is read in the same way as before, but only if there is an external trigger pulse (the threshold register is ignored). Information from channels 2 and 3 (also 128 samples from each one) are automatically read when channel 1 is triggered.

In order to synchronize the readout through the USB port, four control bytes have been implemented for each data block. Two of them, containing the values 1 and 2, indicate the beginning of a data block. The other two, containing the values 3 and 4, indicate the end of a complete data block. This mechanism avoids the transferring of corrupt data, since for each readout operation the control software checks the position of the control bytes. Figure 9 illustrates how the data block is organized. It should be noticed that channel 1, used to digitize the PMT pulses, is read with higher resolution than the other two, which only monitor a slowly varying DC level.

POSITION INDEX	DESCRIPTION	CONTENT (decimal)
1	Header	1
2	Header	2
3	Channel 1, bits [11..4]	sample 1
4	Channel 1, bits [3..0]	sample 1
...	...	...
269	Channel 1, bits [11..4]	sample 134
270	Channel 1, bits [3..0]	sample 134
271	Channel 2	sample 1
272	Channel 2	sample 2
...	...	...
404	Channel 2	sample 134
405	Channel 3	sample 1
406	Channel 3	sample 2
...	...	...
538	Channel 3	sample 134
539	Rate Counter, bits [15..8]	count
540	Rate Counter, bits [7..0]	count
541	Header	3
542	Header	4

* For the three channels, the first six samples are not valid.

Figure 9: The DPM data block map for every detected event

3.3 Characterization results

Data related to the above described circuits performance are summarized in the following figures. The amplifier and shaping circuit was previously simulated and tuned to provide the required gain and bandwidth. Simulated and measured data are shown in Figure 10.

In order to check the rate-meter circuit linearity, we applied to it a varying frequency pulse from a precise pulse generator. The used frequency values covered from few Hz up to few KHz. The results are shown in Figure 11. A linear fit has been done to the data in the region of interest, so that the conversion factor from DC level to count rate is made available. The error bars seen in Figure 11 include, in addition to the electronic noise, the precision of the digital oscilloscope with which the DC-level measurements were done.

The temperature sensor, as previously mentioned, is not very precise and is only meant to provide a rough evaluation of room temperature. It has been calibrated with three temperature values which were cross-checked with an infra-red thermometer. The result is shown in Figure 12. A linear fit has also been done to the region of interest. The wide error bars in the temperature axis are due to instabilities in the used heat sources. In the DC output axis the error bars are multiplied by a factor 10. Since the used thermistor has a slow time response, the circuit output is relatively stable in spite of temperature fluctuations.

The DPM performance in the configuration here required has been characterized by injecting a stable DC level at the input and measuring the fluctuations in the corresponding channel of the analog-
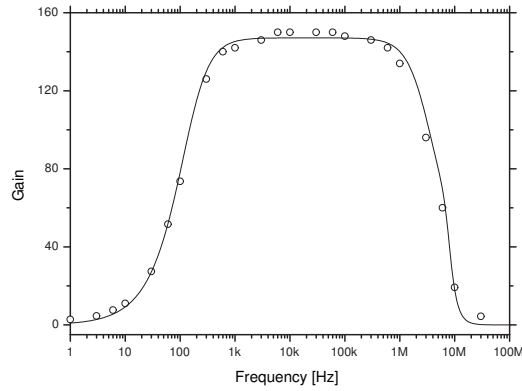
Figure 10: Simulated (continuous line) and measured (circles) data for the amplifier and shaping circuit gain × bandwidth performance
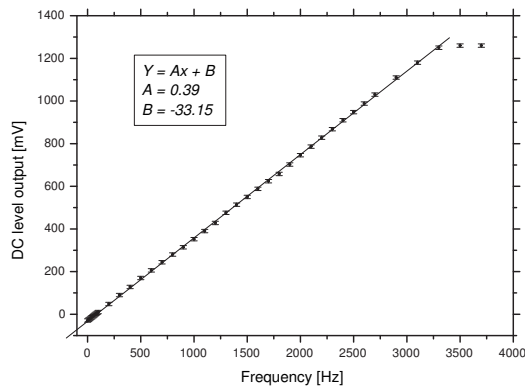

Figure 11: Linear relation between DC-level and input counting rate in the rate-meter circuit
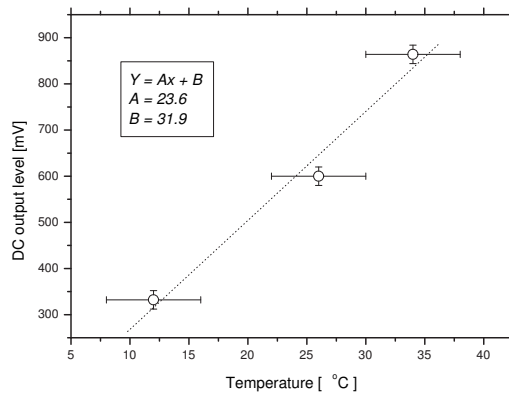

Figure 12: Temperature sensor calibration. The error bars in the DC level axis are multiplied by 10

to-digital converter. Since it works from negative to positive voltage values, both polarities have been used in the measurements. In Figure 13 one may see the relatively good proportionality relating voltage amplitude and ADC channel. The linear fits to the measured data provide conversion factors that are incorporated to the data acquisition software. The error bars are multiplied by a factor 10, so that a slight tendency to increase the conversion error at higher amplitudes is exhibited.
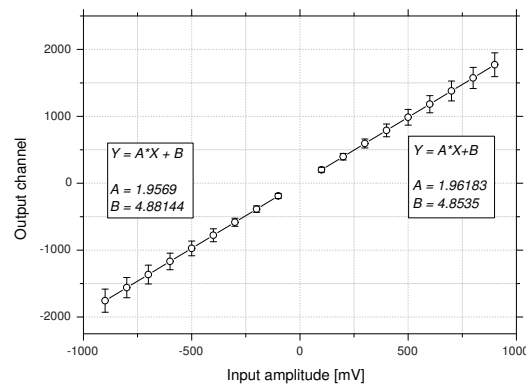

Figure 13: DPM calibration. The error bars are multiplied by 10

4 Conclusion

The first experimental setup for taking data - in the context of the Angra Neutrino Project - from a detector placed near an Angra nuclear reactor has been completed. Although this will not be exactly the one used in the neutrino detector, it represents an important prototype from which much will be learnt and developed. The system will acquire relevant data concerning the local background and may as well be used in other applications - as, for example, cosmic rays measurements - not necessarily in the reactor area.

5 Acknowledgements

References

[1] I. Frank, I. Tamm. Doklady Akademii Nauk SSSR, Vol. 14, 109-14, Seriya A (1937).

[2] R. Machado. Centro Brasileiro de Pesquisas Fsicas, Msc. Thesis (2005).

[3] D. Alexander, K. M. Pathak, M. G. Thompson. J. Phys. A (Proc. Phys. Soc.), Vol. 1, Ser. 2, 578-583 (1968).

[4] I. Alekotte et al. Nucl. Instrum. and Meth. in Phys. Res., A, 586, 409-420 (2008).

[5] P. S. Allison, D. Barnhill. The Auger Project, GAP Note 2004-046 (2004).

[6] A. F. Barbosa. The Angra Neutrino Project, AngraNote 001-2007 (2007).